DOR: 20.1001.1.27170314.2023.12.3.4.1

Research Paper

Effect of Different FGM Models on Creep Analysis of Thick-walled Cylindrical Pressure Vessel

Fakher Abdolkhani[1] , Mohammad Hashemian[1*], Farshid Aghadavoudi[1], Nabard Habibi[2]
[1]Department of Mechanical Engineering, Khomeinishahr Branch, Islamic Azad University, Khomeinishahr, Iran
[2]Department of Mechanical Engineering, Faculty of Engineering, University of Kurdistan, 6617715175, Sanandaj, Iran
[*]Email of Corresponding Authors: hashemian@iaukhsh.ac.ir
Received: August 28, 2023; Accepted: October 19, 2023

Abstract
Thick-walled cylindrical vessels are used widely in petrochemical and power plants. New additive manufacturing technology has made it possible to make FGMs. This research studies the creep analysis in the cylindrical FGM pressure vessel by considering three models and yield criteria. Also, the governing equations were extracted by considering the FGM models, and for determining creep stresses, the partial differential equations, were solved. Norton's equation is used to determine creep strain rates. The advantage of the exponential model is that in the inner radius for all n radial and circumferential creep strains rates have a constant value that is maintained by increasing the internal pressure up to 400 MPa. The graphs are smooth, and their values tend to zero in the outer radius. The changes of creep strain rate in terms of n in different internal pressures for the exponential model in the inner radius of the vessel show that increasing n from -4 to 0, these parameters have a reduction to the form of an exponential function, and the slope of the graph has the highest value at 360 MPa.

Keywords
Creep, Radial Stress, Pressure Vessel, FGM

1. Introduction

Thick-walled pressure vessels are used widely in power plants and petrochemical industries. Universal application of these vessels includes high-pressure reactor vessels used in metallurgical operations, power plants, air compressor units, pneumatic reservoirs, hydraulic tanks, storage for gases like butane LPG, etc. [1]. In the pressure vessel and piping, creep deformation continued as the key design consideration. Also, creep deformation is considered a significant failure mode [2]. In addition, according to classical design, creep analysis should be considered for the design and manufacturing of structures and vessels that work at high temperatures and constant loads. The accurate prediction of creep life plays a key role in the structural integrity of high-temperature elements. Continuum damage mechanics can be applied in conjunction with FE analysis to provide a fundamental step in modeling creep failure [3]. Mao et al. [4] investigated creep and damage analysis of reactor pressure vessels considering the core meltdown scenario. An advanced model was shown

to analyze the fracture time and fracture position of the pressure vessel under an internally heated melt pool.

Kevin et al.[5] creep response of Alloy 617 (this Alloy is an austenitic, solution-strengthened nickel-based superalloy currently being pursued by the nuclear industry as an intermediate heat exchanger structural material for high-temperature Reactors). Also, they evaluated the accuracy of three established creep damage models in predicting the creep time-to-failure and strain-to-failure in the temperature range of 800-1000°C.

The cylinders are widely used and subjected to mechanical and thermal loading. In recent years, researchers have sought to solve nonlinear equations governing cylinders analytically and semi-analytically, considering new advanced materials such as Functionally graded materials (FGMs) and nanocomposite [6]. FGMs are a new generation of composites that are nonhomogeneous in microscopic terms and structural characteristics, including material distribution and phase size, which change gradually from one surface to another surface.

Modern additive manufacturing processes to produce gradient metallic materials have expanded the application of FGMs. In the exponential model, the material profile is unique and it is not possible to define an FGM with the desired structure [6]. Habibi et al. [6] investigated the analysis of mechanical properties, and electrical potential of an FGM thick hollow cylinder that has piezoelectric property under mechanical and thermal loads. Distribution of the mechanical property of the material is considered in terms of the radius using the power distribution function.

Hourari et al. [7] investigated the numerical prediction of the mechanical behavior up to the damage of the bends of the FGM-type ceramic/metal pipes. The results were presented in the form of force–displacement curve. The analysis considered the effect of the main parameters in a bent FGM pipe under internal pressure and bending moment on the variation of the force–strain curves.

In another research [8], the creep of thick-walled cylindrical vessels made of FGM with autofrettaged treated was investigated using the analytical method. In the equivalent stress diagram, the resulting stress at the plastic points of the vessel reaches the yield stress of the FGM, and the stress decreases along the radius. The results show that up to a dimensionless plastic depth of 1.5, the change in residual strain rate is negligible.

Samiha et al. [9] developed an analytical formulation of shrink-fitted FGM axisymmetric thick-walled cylinders based on the linear plane elasticity theory. The results show that the variation of the FGM composition has a clear effect on the fit pressure in the intersection area of the two fitted cylinders. The value of this pressure affects the distribution of radial and tangential stresses in the FGM cylinder walls.

Sklepus [10] investigated the problem of creep of FGM hollow cylinders and complex-shaped bodies of revolution. For the variational statement of the problem, a Lagrangian-form functional defined for kinematically admissible velocities is used. A numerical analytical method for solving the nonlinear initial–boundary-value creep problem is developed. The creep of the material is described by the Norton law. Also, the Young modulus and the creep characteristics of the material depend on the volume fraction of the reinforcing material.

The composition evaluation of FGMs is a concern of a designer to enhance the proper functioning of these materials that adopt them in industrial applications [11]. Habibi et al. [12] presented a semi-analytical method for estimating steady-state creep and elastic behavior in FGM rotary cylinders.

They assumed the cylinder was divided into numerous finite-width layers with constant thermodynamic properties in each layer. Radial and circumferential strains change (dimensionless stains) in terms of the radius illustrated for a different power of FGM for different temperatures and limited timeframe. Thermal analyses of a radially thick-walled FG spherical vessel and an infinite cylindrical vessel were conducted analytically by the steady-state 1D Fourier heat conduction theory under Dirichlet's boundary conditions [13]. Employing an FGM power model, differential equations were obtained in the form of Euler-Cauchy types. Three pairs of physical metal-ceramic were selected to study the effect of the aspect ratio (as the inner radius to the outer radius of the structure) on the temperature and heat flux variation along the radial coordinate. Then a parametric study is performed with hypothetic inhomogeneity indexes for varying aspect ratios.

Time-dependent creep and stress redistribution analysis of thick-walled FGM spheres under internal pressure and a uniform temperature field was investigated [14]. They assumed the mechanical properties in terms of radius obeyed the simple power law. A general solution for 1D steady-state thermal and mechanical stresses in a hollow thick-walled cylinder made of an FGM was obtained by a novel approach [15]. The temperature distribution was considered as a function of radius, with general thermal and mechanical boundary conditions on the inside and outside surfaces of the cylinder. The material properties, except Poisson's ratio, are assumed to be exponentially varying through the thickness.

Kalali et. al [16] obtained an elastoplastic stress solution in the axisymmetric problems of the rotating disk. In their research, the rotating disk was made of ceramic/metal FGMs. They assumed that the material's plastic deformation follows an isotropic strain-hardening rule based on the Von-Mises yield criterion. The mechanical properties of the graded material were modeled by the modified rule of mixtures. The analysis of mechanical and thermal stresses for a long hollow FGM cylinder as functions of radial and longitudinal directions is developed [17]. The material properties are graded along the radial direction according to the power functions of the radial direction.

The study of Jacob [18] evaluated the influence of radial body forces on FGM and non-FGM pressure vessels. It contains an extensive overview of pressure vessels made from both kinds of material. Also, the mathematical development of the stress-strain field in the model is influenced by the body forces performed. Besides, a new power-law model for FGM materials has been suggested and discussed. The study investigates steady-state creep in a rotating Al-SiCp disc having different thickness profiles and reinforcement (SiCp) gradients [19]. The disc material is assumed to creep according to threshold-stress-based law and yield following the Tresca criterion. The stress and strain rates in the disc were estimated utilizing solving the disc equilibrium equation with creep fundamental equations.

In the other research, Smaisim et al. [20] reviewed the thermoelastic and creep properties of functionally graded cylindrical shells, which have shown superior performance under thermo-mechanical loads. The review covers governing equations, and analysis of works conducted and suggests that further research is needed to explore their creep properties under different loading conditions.

Kiarasi et al. [21] attempted to improve the mechanical properties and creep behavior of the magnesium alloy Mg–9Al–1Zn (AZ91) in three different stress levels. They investigated experimentally the addition effects of different values of yttrium oxide nanoparticles to the AZ91.

The results revealed that the addition of yttrium oxide (Y2O3) nanoparticles increases the strength of AZ91 magnesium alloy until the nanoparticles do not clump in the microstructure.

In a new study, the effect of friction and rotational speed parameters changes on the transient thermoelastic response of a rotating functionally graded cylinder with a short length under thermal and mechanical loads are studied based on the first-order shear deformation theory (FSDT) by Dehkourdi et al. [22]. The results show that these changes have significant effects on the measured parameters and in many industrial applications, these coefficients are not constant during the work period and have changed.

In the newest research, Seddighi et al. [23] presented the creep analysis in a thick-walled cylinder under internal pressure and heat flux at the inner and outer surfaces based on the first-order shear deformation theory and the thermal field is assumed two-dimensional through the thickness and along cylinder whose in radial direction the thermal field is considered linear. The effects of parameters such as pressure, heat flux, and radial displacement at different temperatures on stress distribution have been discussed.

According to a review of the previous studies, it is concluded that creep analysis in FGM cylindrical pressure vessels, considering different FGM models has not been covered yet. This research studies the creep analysis in the cylindrical pressure vessel by considering FGM models (exponential, power series, and modified power) and yield criteria such as Von Mises and Tresca.

The equilibrium and compatibility equations governing the thick-walled cylindrical pressure vessel in polar coordinates are as follows:

$$\frac{d\sigma_r}{dr}+\frac{\sigma_r-\sigma_\theta}{r}=0, \tag{1}$$

$$\frac{d\varepsilon_\theta}{dr}+\frac{\varepsilon_\theta-\varepsilon_r}{r}=0, \tag{2}$$

where $\sigma_r,\ and\ \sigma_\theta$ are radial and Circumferential stresses, also, $\varepsilon_r,\ and\ \varepsilon_\theta$ are circumferential and radial strains. The following equations can be concluded under the conditions of plane strain.

$$\varepsilon_r=\frac{1}{E(r)}\{\sigma_r-v(\sigma_z+\sigma_\theta)\}, \tag{3}$$

$$\varepsilon_\theta=\frac{1}{E(r)}\{\sigma_\theta-v(\sigma_z+\sigma_r)\}, \tag{4}$$

$$\varepsilon_z=\frac{1}{E(r)}\{\sigma_z-v(\sigma_r+\sigma_\theta)\},\quad \varepsilon_z=0 \quad \Rightarrow \quad \sigma_z=v(\sigma_r+\sigma_\theta), \tag{5}$$

Therefore, circumferential, and radial strains are as follows:

$$\varepsilon_r=\frac{1}{E(r)}\{(1-v^2)\sigma_r-v(1+v)\sigma_\theta\}, \tag{6}$$

$$\varepsilon_\theta = \frac{1}{E(r)}\{(1-v^2)\sigma_\theta - v(1+v)\sigma_r\}, \quad (7)$$

In the present study, the Poisson's ratio (v) is considered constant and equal to 0.3. By placing radial and circumferential strains in the compatibility equation and using the equilibrium equation after simplification, we can write:

$$\frac{d}{dr}\left\{\frac{-v\sigma_r}{E(r)} + \frac{(1-v)\sigma_\theta}{E(r)}\right\} + \frac{(1+v)}{E(r)}\frac{d\sigma_r}{dr} = 0, \quad (8)$$

In this differential equation, the modulus of elasticity, $E(r)$. is a function of the radius of the pressure vessel. After simplifying equation (8), finally

$$-v\left\{\frac{d\sigma_r}{dr} - \frac{dE(r)}{dr}\frac{\sigma_r}{E(r)}\right\} + (1-v)\left\{\frac{d\sigma_\theta}{dr} - \frac{dE(r)}{dr}\frac{\sigma_\theta}{E(r)}\right\} + \frac{d\sigma_r}{dr} = 0, \quad (9)$$

The derivative of the equilibrium equation concerning Θ gives $\frac{d\sigma_\theta}{dr} = \frac{d\sigma_r}{dr} + r\frac{d^2\sigma_r}{dr^2}$, therefore,

$$-v\left\{\frac{d\sigma_r}{dr} - \frac{dE(r)}{dr}\frac{\sigma_r}{E(r)}\right\} + (1-v)\left\{r\frac{d^2\sigma_r}{dr^2} + \frac{d\sigma_r}{dr} - \frac{1}{E(r)}\frac{dE(r)}{dr}\left(r\frac{d\sigma_r}{dr} + \sigma_r\right)\right\} + \frac{d\sigma_r}{dr} = 0, \quad (10)$$

By considering radial and circumferential strains in terms of radial displacement (u_r), we can write equations (6) and (7) in terms of u_r.

$$\varepsilon_r = \frac{du_r}{dr} = \frac{1}{E(r)}\{(1-v^2)\sigma_r - v(1+v)\sigma_\theta\}, \quad (11)$$

$$\varepsilon_\theta = \frac{u_r}{r} = \frac{1}{E(r)}\{(1-v^2)\sigma_\theta - v(1+v)\sigma_r\}, \quad (12)$$

From equations (11) and (12), the following set of two unknown equations is obtained, which can be solved by the Kramer method.

$$\begin{cases}(1-v^2)\sigma_r - v(1+v)\sigma_\theta = E(r)\dfrac{du_r}{dr} \\ -v(1+v)\sigma_r + (1-v^2)\sigma_\theta = E(r)\dfrac{u_r}{r}\end{cases}, \quad (13)$$

$$\sigma_r = \frac{\Delta_{\sigma_r}}{\Delta} = E(r)\frac{\left\{(1-v)\frac{du_r}{dr} + v\frac{u_r}{r}\right\}}{(1+v)(1-2v)}, \quad (14)$$

$$\sigma_\theta = \frac{\Delta_{\sigma_\theta}}{\Delta} = E(r)\frac{\left\{(1+v)\frac{u_r}{r} + v\frac{du_r}{dr}\right\}}{(1+v)(1-2v)}, \quad (15)$$

2.1 Models of FGMs

To compare the effect of the type of FGM model on the stress distribution in the thick-walled cylindrical pressure vessel under internal pressure, three different models (exponential, power, and

modified power models) have been investigated. In this research, the value of the ratio of internal to external radius of the vessel (a/b) is considered equal to m.

- Power Model

In the power model, the modulus of elasticity is considered to form $E(r) = E_0(\frac{r}{a})^n$, where a is the internal radius of the vessel. Also, $\frac{dE(r)}{dr} = \frac{n}{r}E(r)$, and by placing it in the equation (10) after simplification, the Cauchy-Euler differential equation is obtained, which by changing variable $r = e^t \ \ or \ \ t = lnr$ becomes the differential equation with constant coefficients.

$$r^2\frac{d^2\sigma_r}{dr^2} + (3-n)r\frac{d\sigma_r}{dr} + \frac{(2v-1)n}{(1-v)}\sigma_r = 0, \tag{16}$$

$$\frac{d}{dr} = \frac{d}{dt}\frac{dt}{dr} = \frac{d}{dt}\frac{1}{r} \quad \Rightarrow \quad r\frac{d}{dr} = \frac{d}{dt} \quad \Rightarrow r\frac{d\sigma_r}{dr} = \frac{d\sigma_r}{dt}, \tag{17}$$

$$\frac{d^2}{dr^2} = \frac{d}{dr}\left(\frac{d}{dr}\right) = \frac{d}{dt}\left(\frac{d}{dt}\frac{1}{e^t}\right)\frac{dt}{dr} = \frac{1}{r^2}\left(-\frac{d}{dt} + \frac{d^2}{dt^2}\right) \ \Rightarrow \ r^2\frac{d^2\sigma_r}{dr^2} = \frac{d^2\sigma_r}{dt^2} - \frac{d\sigma_r}{dt}, \tag{18}$$

By incorporating equations (17) and (18) in the differential equation (16) and simplifying the following equation is obtained.

$$\frac{d^2\sigma_r}{dt^2} + (2-n)\frac{d\sigma_r}{dt} + \frac{(2v-1)n}{(1-v)}\sigma_r = 0, \tag{19}$$

By writing the characteristic equation to form $t^2 + (2-n)t + \frac{(2v-1)n}{(1-v)} = 0$, the general response of the differential equation is obtained as follows.

$$t = \left(\frac{n}{2} - 1\right) \pm \sqrt{\left(1 - \frac{n}{2}\right)^2 + \frac{(2v-1)n}{(1-v)}} \quad \rightarrow \quad \sigma_r = C_1 r^{t_1} + C_2 r^{t_2}, \tag{20}$$

The boundary conditions are considered as $\sigma_r(r=a) = -p_i$ and $\sigma_r(r=b) = 0$, so the general response constants are obtained as follows.

$$C_1 = \frac{p_i}{b^{t_1}(m^{t_2} - m^{t_1})} \ , \ C_2 = -\frac{p_i}{b^{t_2}(m^{t_2} - m^{t_1})}, \tag{21}$$

By placing the constants in the general response, the dimensionless radial stress is determined as follows.

$$\overline{\sigma}_r = \frac{\sigma_r}{p_i} = \frac{\left(\frac{r}{b}\right)^{t_1} - \left(\frac{r}{b}\right)^{t_2}}{m^{t_2} - m^{t_1}}, \tag{22}$$

By substituting radial stress in the equilibrium equation of the vessel, the dimensionless circumferential stress becomes as follows.

$$\sigma_\theta = r\frac{d\sigma_r}{dr} + \sigma_r \rightarrow \overline{\sigma}_\Theta = \frac{\sigma_\theta}{p_i} = \frac{(1+t_1)\left(\frac{r}{b}\right)^{t_1} + (1+t_2)\left(\frac{r}{b}\right)^{t_2}}{m^{t_2} - m^{t_1}}, \tag{23}$$

- *Exponential Model*

In the exponential model, the modulus of elasticity is considered to form $E(r) = E_0 e^{nr}$, where *n* is constant, and *r* is the radius along with the thickness of the vessel.

By substituting $\frac{dE(r)}{dr} = nE(r)$ and equations of (14) and (15) into the equilibrium equation of vessel, and $\frac{v}{1-v} = v_1$. finally, the second-order differential equation is obtained with variable coefficients, which can be solved by using the power series method.

$$r^2 \frac{d^2u_r}{dr^2} + (1+nr)r\frac{du_r}{dr} + (v_1 nr - 1)u_r = 0, \tag{24}$$

In this model, *n*=1, 2, 3, and *v* = 0.3. For solving the equation, the radial displacement is considered as follows.

$$u_r = \sum_{j=0}^{\infty} a_j r^{j+s} \ , \frac{du_r}{dr} = \sum_{j=0}^{\infty} a_j (j+s) r^{j+s-1}, \ \ \frac{d^2u_r}{dr^2} = \sum_{j=0}^{\infty} a_j (j+s)(j+s-1) r^{j+s-2} \ ,$$

By substituting u_r, $\frac{du_r}{dr}$ and $\frac{d^2u_r}{dr^2}$ in equation (24), after simplification we will have:

$$\sum_{\beta=0}^{\infty} a_\beta \Big[\begin{matrix} (\beta+s)(\beta+s-1) + (\beta+s-1) \\ +v_1 n(\beta+s-1) - 1 \end{matrix} \Big] r^{\beta+s} = 0, \tag{25}$$

By considering $\beta = 0$. then $s(s-1) + (s-1) + v_1 n(s-1) - 1 = 0$, therefore.

$$s^2 + v_1 ns - (v_1 n + 2) = 0. \quad \Delta = (v_1 n + 2)^2 + 4 > 0 \quad \rightarrow \quad s_{1.2} = \frac{-v_1 n \pm \sqrt{\Delta}}{2},$$

As a result, the radial displacement and its derivative relative to the radius are written as follows.

$$s = -\frac{v_1 n}{2} \pm \sqrt{\left(\frac{v_1 n}{2} + 1\right)^2 + 1} \rightarrow \quad u_r = C_1 r^{s_1} + C_2 r^{s_2}, \tag{26}$$

$$\frac{du_r}{dr} = C_1 s_1 r^{s_1 - 1} + C_2 s_2 r^{s_2 - 1} \tag{27}$$

By incorporating equations (26) and (27) in the equations (22) and (23), radial and circumferential stresses are obtained as follows.

$$\sigma_r = \frac{E(r)}{(1+v)(1-2v)} \left\{ C_1 r^{s_1 - 1} \big((1-v)s_1 + v \big) + C_2 r^{s_2 - 1} \big((1-v)s_2 + v \big) \right\}, \tag{28}$$

$$\sigma_\theta = \frac{E(r)}{(1+v)(1-2v)} \{ C_1 r^{s_1} (1 - v + v s_1) + C_2 r^{s_2} (1 - v + s_2 v) \}, \tag{29}$$

Considering the boundary conditions $\sigma_r(r=a) = -p_i$ and $\sigma_r(r=b) = 0$. We will have:

$$C_1 = \frac{-1}{(m^{s_2} - m^{s_1})}\left\{\frac{p_i(1+v)(1-2v)}{E(r)b^{s_1}\left(v + \frac{s_1}{r}(1-v)\right)}\right\}, \quad (30)$$

$$C_2 = \frac{1}{(m^{s_2} - m^{s_1})}\left\{\frac{p_i(1+v)(1-2v)}{E(r)b^{s_2}\left(\frac{v}{r} + \frac{s_2}{r}(1-v)\right)}\right\}, \quad (31)$$

Therefore, by placing these constants in stress equations, the dimensionless radial and circumferential stresses can be determined from the following equations.

$$\overline{\sigma}_r = \frac{\sigma_r}{p_i} = \frac{1}{m^{s_1-1} - m^{s_2-1}}\left\{\left(\frac{r}{b}\right)^{s_1-1} - \left(\frac{r}{b}\right)^{s_2-1}\right\}, \quad (32)$$

$$\overline{\sigma}_\theta = \frac{\sigma_\theta}{p_i} = \frac{b}{m^{s_1-1} - m^{s_2-1}}\left\{\left\{\left(\frac{r}{b}\right)^{s_2} - \left(\frac{r}{b}\right)^{s_1}\right\}\right\}, \quad (33)$$

- *Modified Power Model*

In the modified power model, the modulus of elasticity is considered as $E(r) = \frac{E_0}{2}\left\{(\frac{r}{a})^n + (\frac{r}{b})^n\right\}$, where n is constant and r $(a \le r \le b)$ is the radius along with the thickness of the vessel. By substituting $\frac{dE(r)}{dr} = \frac{n}{r}E(r), \frac{2v-1}{1-v} = v_1$ and equation (14) and (15) into the equilibrium equation of the vessel, the Cauchy-Euler differential equation is obtained. By changing variable $r = e^t \ or \ t = lnr$, the differential equation with constant coefficients is obtained. The characteristic equation for this equation is written as equation (35) which is easily determined by the delta method.

$$r^2\frac{d^2\sigma_r}{dr^2} + (2-n)r\frac{d\sigma_r}{dr} + v_1 n\sigma_r = 0, \quad (34)$$

$$\frac{d^2\sigma_r}{dt^2} + (1-n)\frac{d\sigma_r}{dt} + v_1 n\sigma_r = 0,$$
$$t^2 + (1-n)t + v_1 n = 0\,,$$
$$\Delta = (1-n)^2 - 4v_1 n,$$
$$v_1 = \frac{2v-1}{1-v} = -0.7559 \ \rightarrow \ \Delta > 0, \quad (35)$$
$$t_1 = \frac{1}{2}\left\{n - 1 + \sqrt{(1-n)^2 - 4v_1 n}\right\},$$
$$t_2 = \frac{1}{2}\left\{n - 1 - \sqrt{(1-n)^2 - 4v_1 n}\right\},$$

$$\sigma_r = C_1 r^{t_1} + C_2 r^{t_2}, \quad (36)$$

The boundary conditions are considered as $\sigma_r(r=a)=-p_i$ and $\sigma_r(r=b)=0$, so the general response constants are obtained as follows:

$$\sigma_r=\frac{p_i}{b^{t_1}(m^{t_2}-m^{t_1})}r^{t_1}-\frac{p_i}{b^{t_2}(m^{t_2}-m^{t_1})}r^{t_2}, \tag{37}$$

Therefore, the dimensionless radial stress can be determined from the following equations:

$$\overline{\sigma}_r=\frac{\sigma_r}{p_i}=\frac{1}{m^{t_2}-m^{t_1}}\left\{\left(\frac{r}{b}\right)^{t_1}-\left(\frac{r}{b}\right)^{t_2}\right\}, \tag{38}$$

By substituting radial stress in the equilibrium equation of the vessel, the dimensionless membrane stress becomes as follows.

$$\sigma_\theta=r\frac{d\sigma_r}{dr}+\sigma_r\rightarrow\ \overline{\sigma}_\Theta=\frac{\sigma_\theta}{p_i}=\frac{1}{m^{t_2}-m^{t_1}}\left\{(1+t_1)\left(\frac{r}{b}\right)^{t_1}+(1+t_2)\left(\frac{r}{b}\right)^{t_2}\right\}, \tag{39}$$

2.2 Creep in Vessel

Creep is an important material behavior occurring at elevated temperatures, especially at that higher than 50% of the melting temperature of the material. It is the time-dependent, inelastic deformation that takes place when the material is subjected to a load over time. A structure changes the state of stress and strains, reduction in material strength, etc. The deformation is commonly characterized in the form of strain versus time data, known as the creep curve [24]. The Modulus of elasticity (E) of the FGM vessel at any radius (r) is evaluated from the rule of the mixture as follows:

$$E(r)=E_dV_d+E_m(1-V_m), \tag{40}$$

Where V_d is the average volume fraction of SiC_p reinforcement in the composite cylinder and E_d (450 GPa) and E_m (69 GPa) are, respectively, the Elastic modulus of SiC_p and Al matrix [25]. The material of the cylinder is assumed to undergo steady-state creep following Norton's law [26-28]:

$$\dot{\varepsilon}=B(r)\bar{\sigma}^{n(r)}, \tag{41}$$

Where $\bar{\sigma}$ is the effective stress given by yield criterion, and $\dot{\varepsilon}$ is the effective strain rate and $B(r)$ and $n(r)$ are the creep parameters at any radius r of the composite vessel that depended on the content of SiC_p [28] in the vessel. These parameters are estimated as follows:

$$B(r)=B_0\left[\frac{V(r)}{V_{ave}}\right]^{\varphi}, \tag{42}$$

$$n(r)=n_0\left[\frac{V(r)}{V_{ave}}\right]^{-\varphi}, \tag{43}$$

where φ is the grading index, and B_0 is the value of creep parameter B for a similar composite vessel but having a uniform distribution of SiC_p equal to V_{ave} over the entire radius. Also, n_0 is the value of stress exponent (n) for a similar composite vessel with a uniform distribution of SiC_p equal to V_{ave} everywhere. By incorporating equations (22), (23), (32), (33), (38), and (39) in equation (41), the dimensionless radial and circumferential creep strains rate for three models is as follows: equations (44) and (45) for exponential model, equations (46) and (47) for power model, and equations (48) and (49) for modified power model.

$$\dot{\varepsilon}_{radial} = \dot{\varepsilon}_r = B\{\frac{\left(\frac{r}{b}\right)^{t_1} - \left(\frac{r}{b}\right)^{t_2}}{m^{t_2} - m^{t_1}}\}^n, \quad (44)$$

$$\dot{\varepsilon}_{circumferential} = \dot{\varepsilon}_\theta = B\{\frac{(1+t_1)\left(\frac{r}{b}\right)^{t_1} + (1+t_2)\left(\frac{r}{b}\right)^{t_2}}{m^{t_2} - m^{t_1}}\}^n, \quad (45)$$

$$\dot{\varepsilon}_{radial} = \dot{\varepsilon}_r = B\{\frac{1}{m^{s_1-1} - m^{s_2-1}}\left\{\left(\frac{r}{b}\right)^{s_1-1} - \left(\frac{r}{b}\right)^{s_2-1}\right\}\}^n, \quad (46)$$

$$\dot{\varepsilon}_{circumferential} = \dot{\varepsilon}_\theta = B\{\frac{b}{m^{s_1-1} - m^{s_2-1}}\left\{\left\{\left(\frac{r}{b}\right)^{s_2} - \left(\frac{r}{b}\right)^{s_1}\right\}\right\}\}^n, \quad (47)$$

$$\dot{\varepsilon}_{radial} = \dot{\varepsilon}_r = B\{\frac{\left(\frac{r}{b}\right)^{t_1} - \left(\frac{r}{b}\right)^{t_2}}{m^{t_2} - m^{t_1}}\}^n, \quad (48)$$

$$\dot{\varepsilon}_{circumferential} = \dot{\varepsilon}_\theta = B\{\frac{(1+t_1)\left(\frac{r}{b}\right)^{t_1} + (1+t_2)\left(\frac{r}{b}\right)^{t_2}}{m^{t_2} - m^{t_1}}\}^n, \quad (49)$$

The equivalent stress is obtained from the Tresca and Von Mises criteria of the following equations:

$$\overline{\sigma}_{\text{Tresca}} = |\overline{\sigma}_\theta - \overline{\sigma}_r|, \quad (50)$$

$$\overline{\sigma}_{\text{Von Mises}} = \sqrt{\overline{\sigma}_\theta{}^2 + \overline{\sigma}_r{}^2 - \overline{\sigma}_\theta\overline{\sigma}_r}, \quad (51)$$

Where; $\overline{\sigma}_\theta, \overline{\sigma}_r$ for dimensionless circumferential and radial stress can be replaced from equations (22), (23), (32), (33), (38), (39) for power, exponential, and modified power models, respectively.

3 Results and Discussion

3.1 Stress Analysis in Vessel

Dimensionless radial and circumferential stresses in terms of dimensionless radius for three models of FGMs are illustrated in Figures 1-3. According to Figure 1*a*, it is observed that for the exponential model, the dimensionless radial stress in the inner and outer radii of the vessel has a constant value for different views of the radial ratio, and with the increase of the value of *n* from -4 to zero, the slope of the graph becomes less and when *n* is equal to zero, the FGM model tends towards homogeneous material. Also, this model creates dimensionless negative radial and circumferential stresses in the vessel wall. According to Figure 4*b*, by increasing the value of *n* from -4 to zero, the amount of radial stress without compressive dimension decreases in the inner radius of the tank, and in the outer radius of the tank, the number of changes in *n* has no effect.

Figures 2*a, and b*, show the changes of the dimensionless radial stress in terms of the dimensionless radius for the power model which are in the form of a decreasing exponential function, and have a positive value in the inner radius and for external radius becomes zero. Also, by increasing the value of *n* towards zero, the dimensionless radial stress decreases, which is significant in the middle thickness of the vessel (dimensionless radius equal to 0.75). According to Figure 2*a*, the changes in dimensionless circumferential stress are in the form of an exponential function of increasing pressure, which is reduced by increasing the value of *n* towards -4, and this stress reduction is significant in the middle thickness of the vessel.

Dimensionless radial and circumferential stresses change in terms of dimensionless radius for the modified power model (Figures 3*a*, *b*) also have a negative value. In dimensionless radial stress, the slope of the graph decreases with the increase of the *n* value from -4 to zero. The changes in the graphs also increase as an exponential function from the side of the inner wall to the outer wall of the vessel. In Figure 3*a*, the circumferential stress has a negative value and in the inner wall of the vessel, it is different for different values of view *n*, and the highest value of compressive stress is related to viewing -4 and with the increase of the dimensionless radius from the inner wall towards the wall externally, this difference decreases.

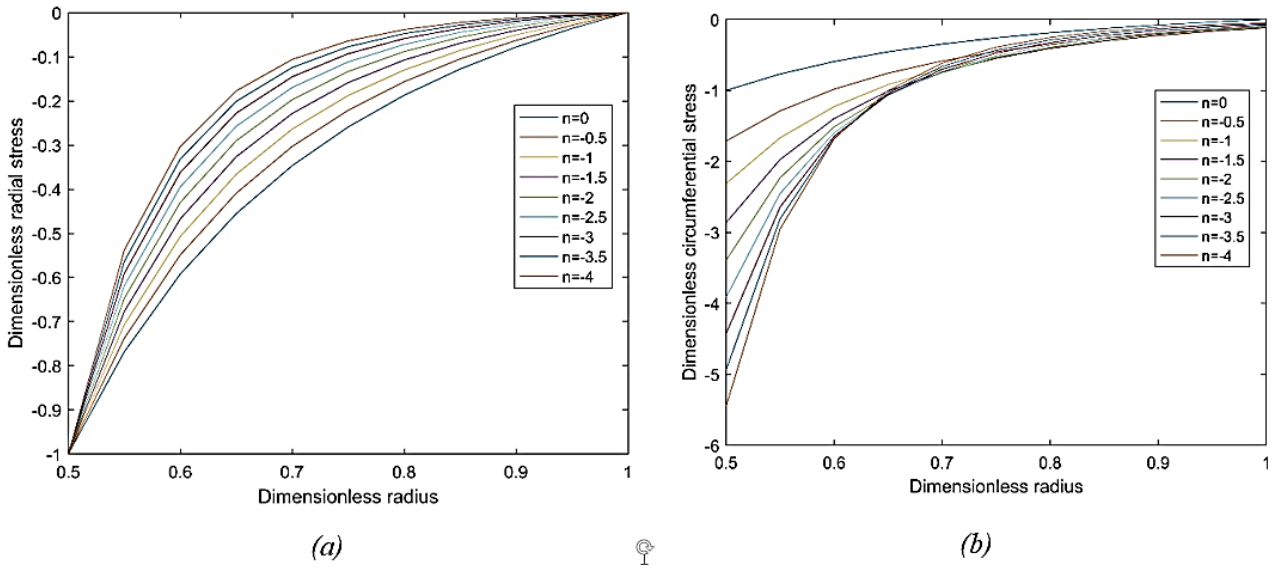

Figure 1. Dimensionless stresses in terms of dimensionless radius, *a*) radial stress, and *b*) circumferential stress (The exponential model)

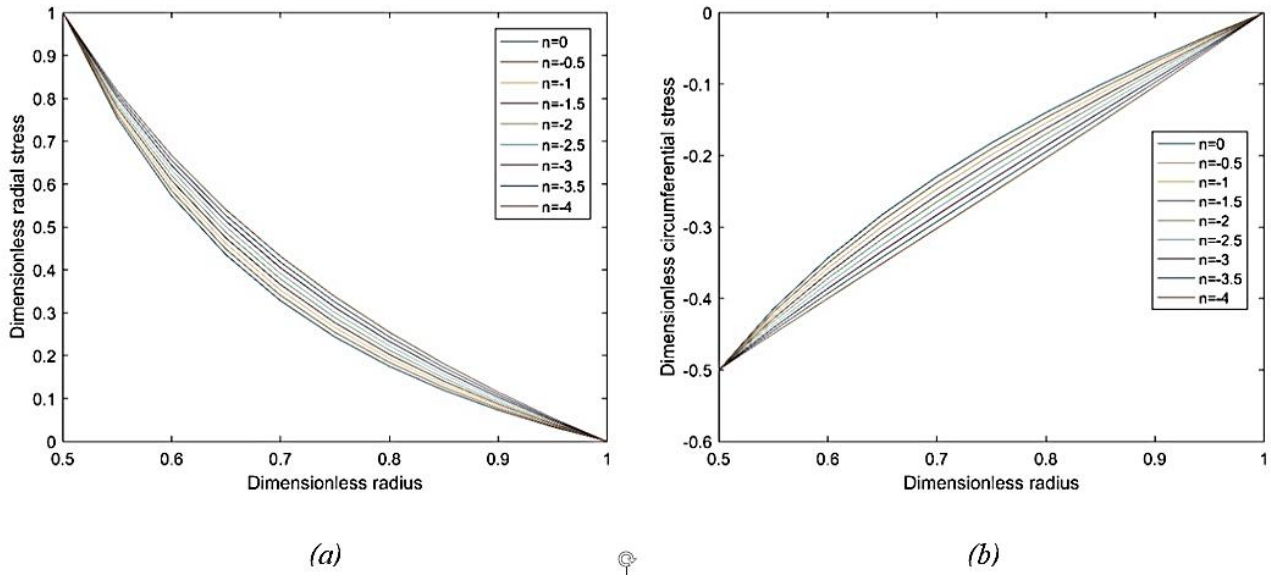

Figure 2. Dimensionless stresses in terms of dimensionless radius, a) radial stress, and b) circumferential stress (The power model)

The dimensionless radial and circumferential stress distribution in terms of the dimensionless radius for all three models, at *n* equal to 4, is shown in Figure 4. According to these graphs, the exponential

and modified power models have close results. The stresses created by these two models in the vessel are the pressure which is the highest value in the inner radius and converges to zero in the outer radius of the vessel. The second FG model also creates radial tensile stress in the vessel wall and a small circumferential compressive stress is created in the vessel.

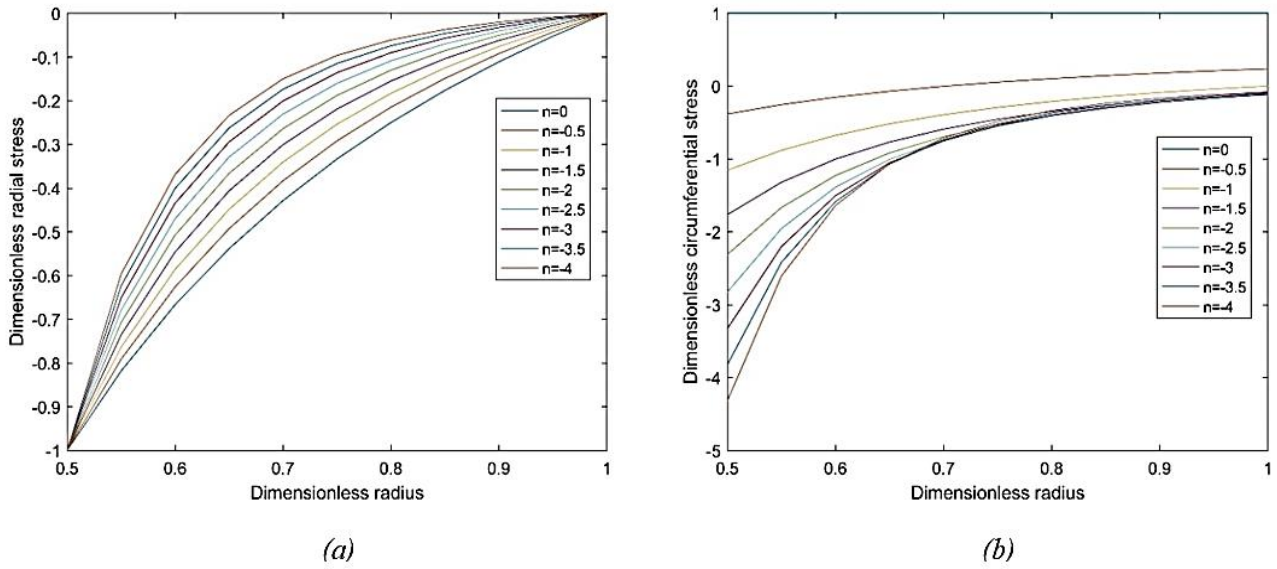

Figure 3. Dimensionless stresses in terms of dimensionless radius, a) radial stress, and b) circumferential stress (The modified power model)

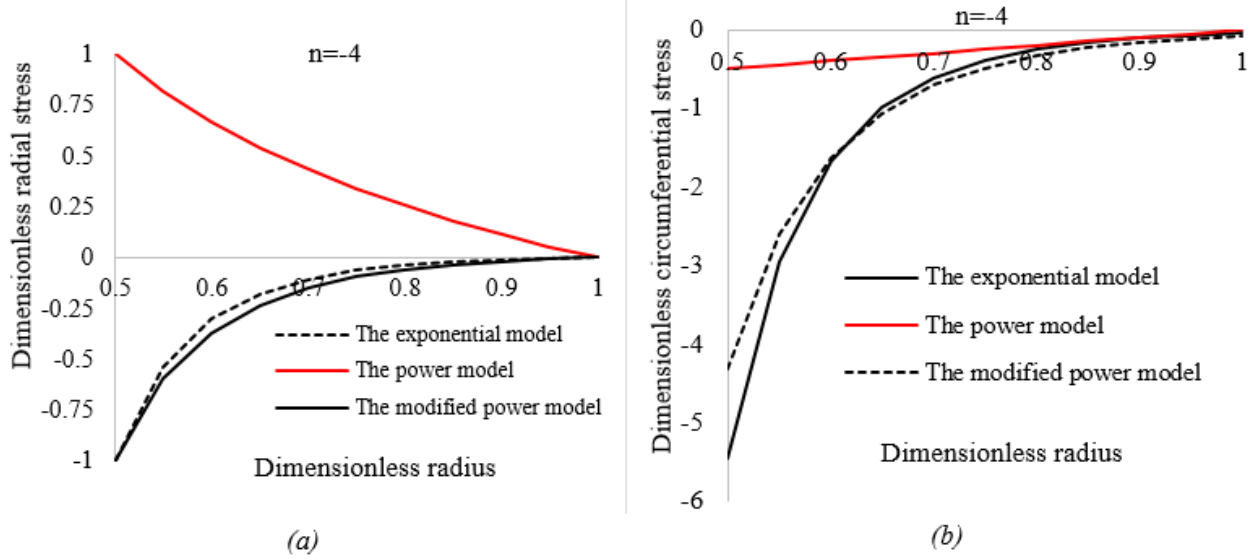

Figure 4. Distribution of dimensionless stresses in terms of dimensionless radius for all three models, a) radial stress, and b) circumferential stress (n= -4)

3.2 Creep Strain Rate Analysis in Vessel

In the Norton equation, the values of B_0, n_0, φ in equations (42), and (43) according to [29], are $2.77 \times 10^{-16}, 3.75, 0.7$, respectively. However, it has been shown that changing these parameters $(B(r), n(r))$ has little effect on the strain rate in Norton's equation [41], so in the present work, these two parameters are considered constant ($B = 4.79 \times 10^{-22}\ MPa^{-6}s^{-1}, n = 6$) [30].

The changes in the rate of creep strains (radial, circumferential) in terms of *n* with different internal pressures for the exponential FG model in the inner radius of the tank can be seen in Figures 5 and 6. According to the graphs, the changes in the rate of circumferential creep, Von Mises, and Tresca strains decrease exponentially with increasing *n* from -4 to zero, and the slope of the graph has the highest value at a pressure of 360 MPa. Also, the rate of creep strains remains constant with the change in pressure. The changes in the rate of creep strains (Von Mises and Tresca) in terms of *n* with different internal pressures for the exponential model for FGM in the inner radius of the vessel are illustrated in Figures 7 and 8. According to the graphs, changes in the rate of circumferential creep, Von Mises, and Tresca strains decrease exponentially with increasing n from -4 to zero, and the slope of the graph has the highest value at a pressure of 360 MPa, and the rate of creep strains remain constant with in terms of pressure.

For the power FGM model and dimensionless average radius, the changes in creep strain rates in terms of *n* with different internal pressures up to 360 MPa are shown in Figures 7 and 8. From these graphs, the changes of these parameters change from a linear form to a decreasing exponential function as the internal pressure of the vessel increases from 40 MPa and n from -4 to zero. Also, the slope of the graphs increases, and they have the lowest value on the outer radius of the vessel.

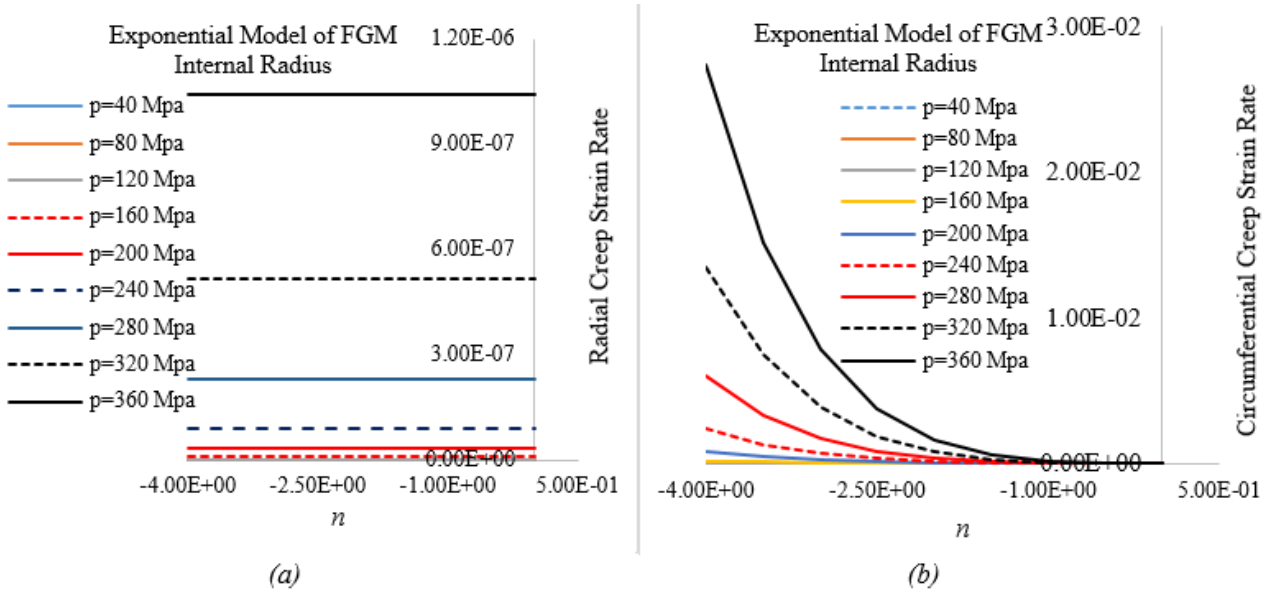

Figure 5. The changes in the rate of creep strains in terms of different internal pressures (MPa), *a*) radial stress, and *b*) circumferential stress (The exponential model and internal radius)

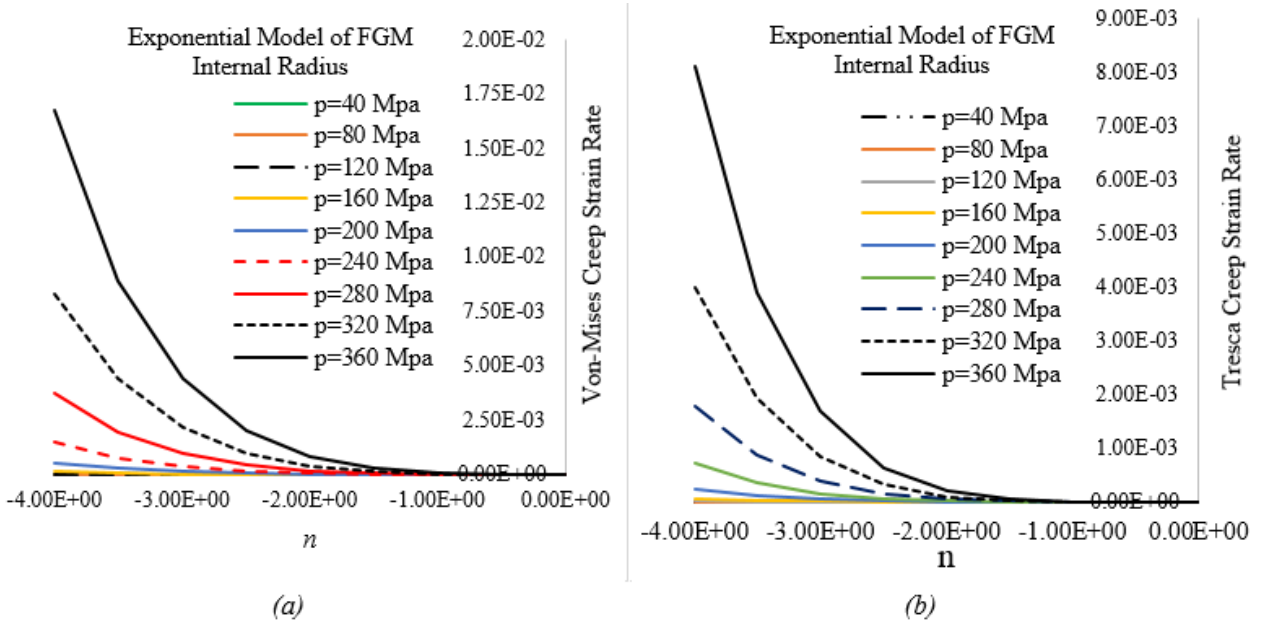

Figure 6. The changes in the rate of creep strains in terms of different internal pressures (MPa), a) Von-Mises, and b) Tresca (The exponential model and internal radius)

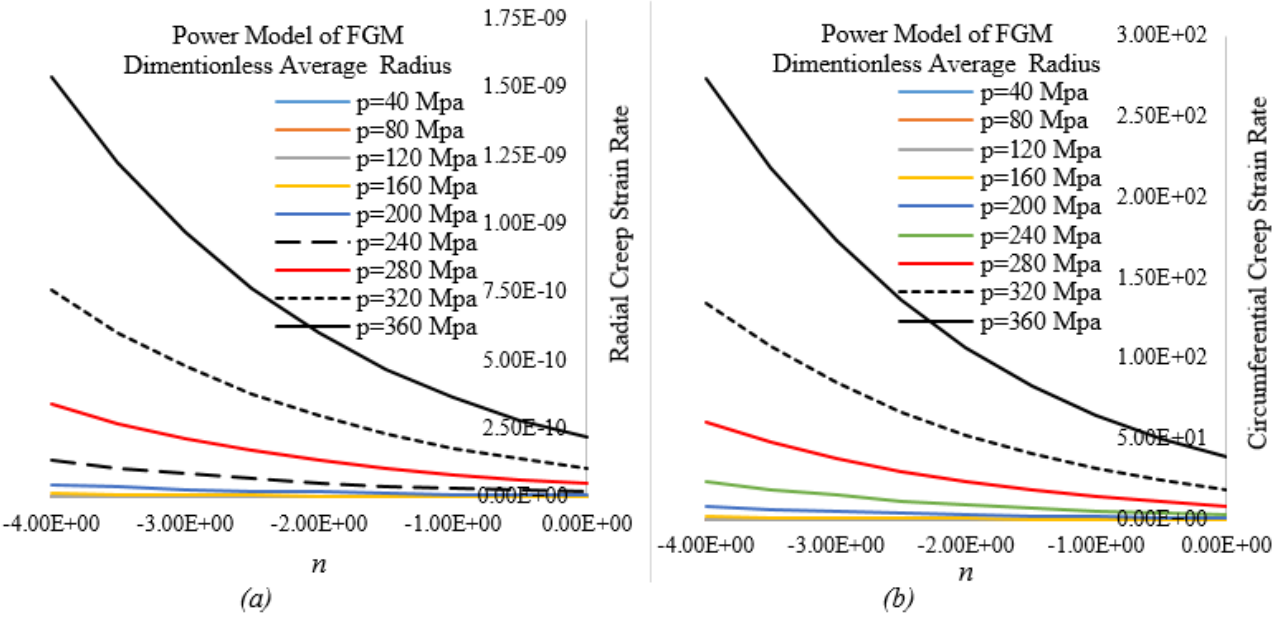

Figure 7. The changes in the rate of creep strains in terms of different internal pressures (MPa), *a*) radial, and *b*) circumferential (The power model and dimensional mean radius)

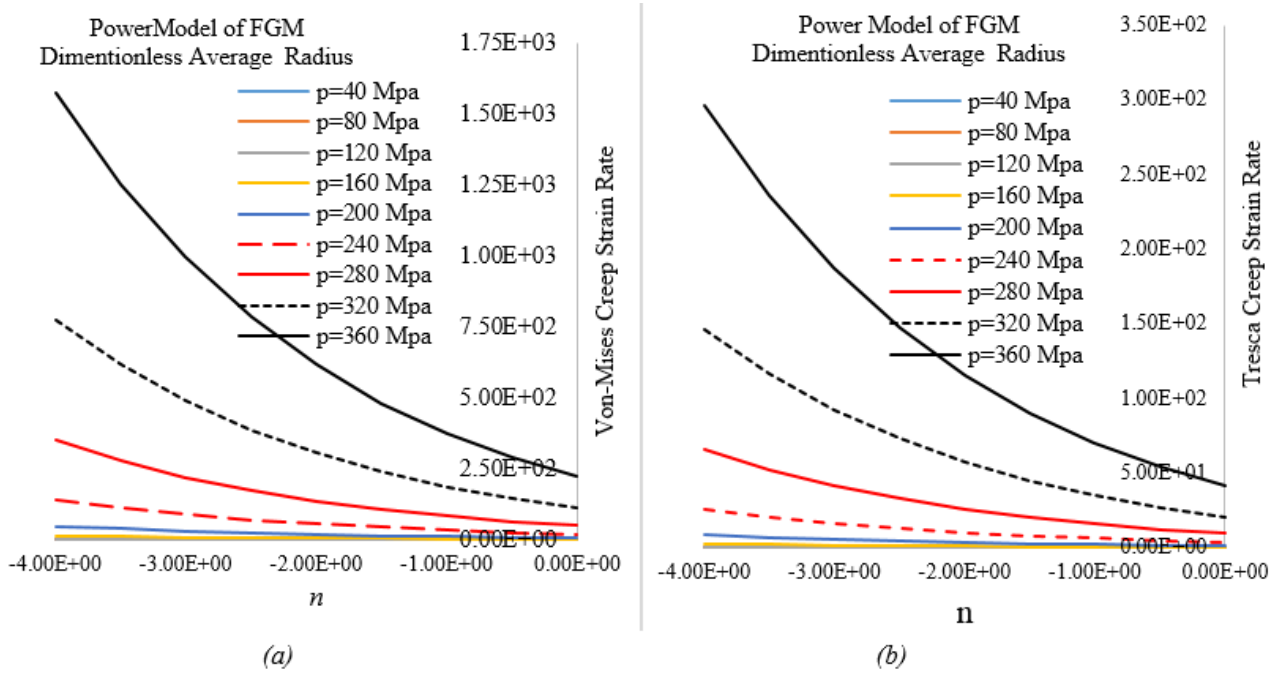

Figure 8. The changes in the rate of creep strains in terms of different internal pressures (MPa), *a*) Von-Mises, and *b*) Tresca (The power model and internal radius)

The changes of the radial and circumferential creep strains rate in terms of dimensionless radius for different *n* and internal pressure equal 400 MPa (all three models) illustrated in Figures 9*a-c* and 10*a-c*. For *n=0*, in all three models, the considered FGM is transformed into a homogeneous state, and an identical solution for the radial creep strain rate is obtained. From the power model, a higher value of the radial creep strain rate is obtained for different *n*. According to these figures observed for dimensionless mean radius, in *n*=-4, the exponential and modified power models, the radial creep strain rates have very small and close values. The effect of *n* in the second model is far less than in the other two models. According to Figure 10*b*, the pressure of 400 MPa has a significant effect on the circumferential creep strain rate in the dimensionless mean radius for the Power model. The value of the circumferential creep strain rate created in the dimensionless mean radius for the exponential and modified power FGM models is much lower than the power model. The changes in the rate of creep strains (radial, circumferential, Von-mises, and Tresca) in terms of dimensionless radius for different internal pressure (40 MPa-400 MPa), *n*=-1.5, and dimensionless mean radius *a*) the exponential model, *b*) the power model, and c) the modified power model) illustrated in Figure 11. According to Figure 11*a, c* is observed that the slope of circumferential creep strain rate curve in the exponential and modified power FGM models for the dimensionless mean radius is much higher than other strain rate curves and compared to the second model, much lower values have been obtained for the strain rates.

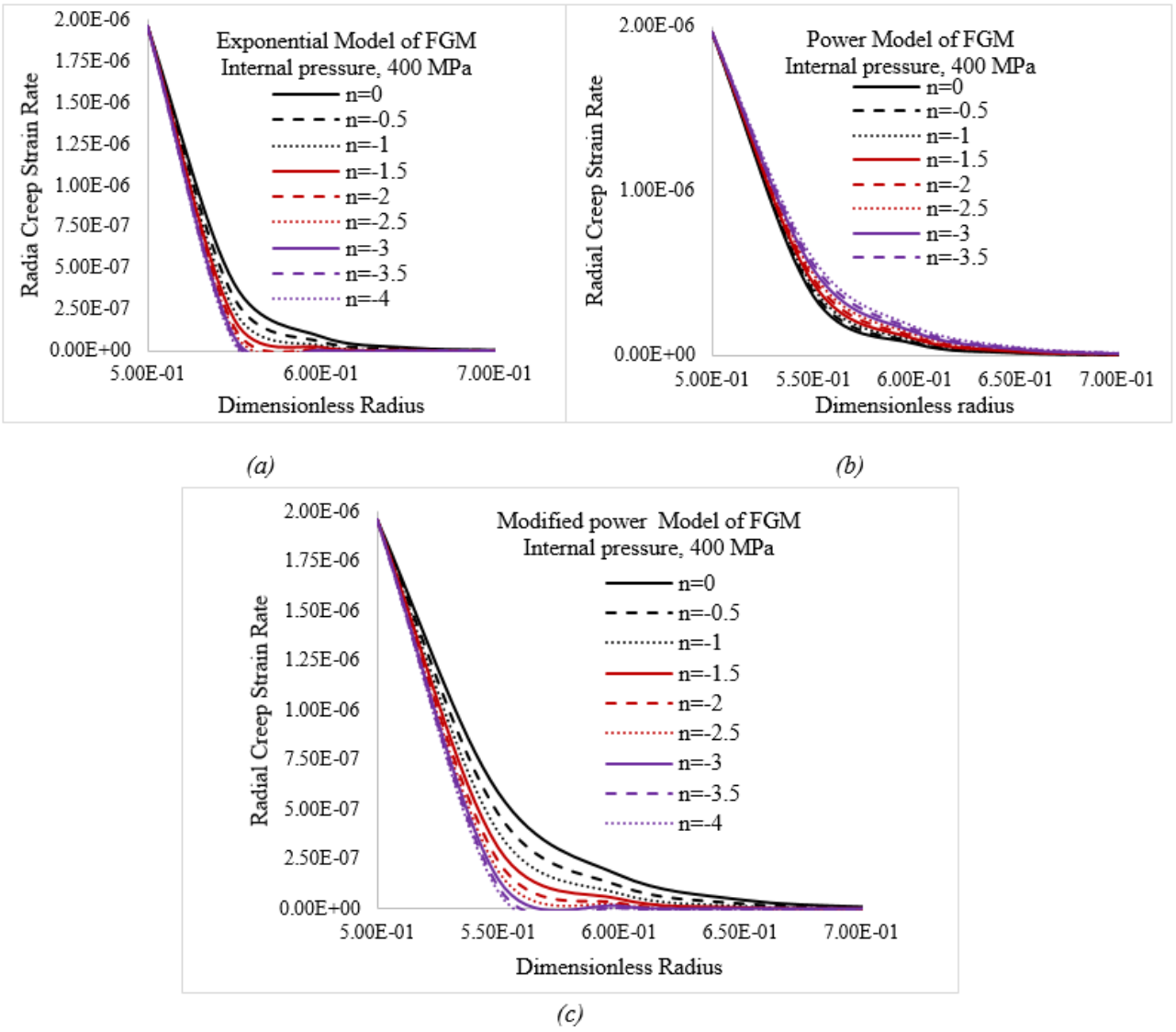

Figure 9. The changes in the rate of radial creep strain in terms of dimensionless radius for different n, a) the exponential model, b) the power model, and c) the modified power model (internal pressure, 400 MPa)

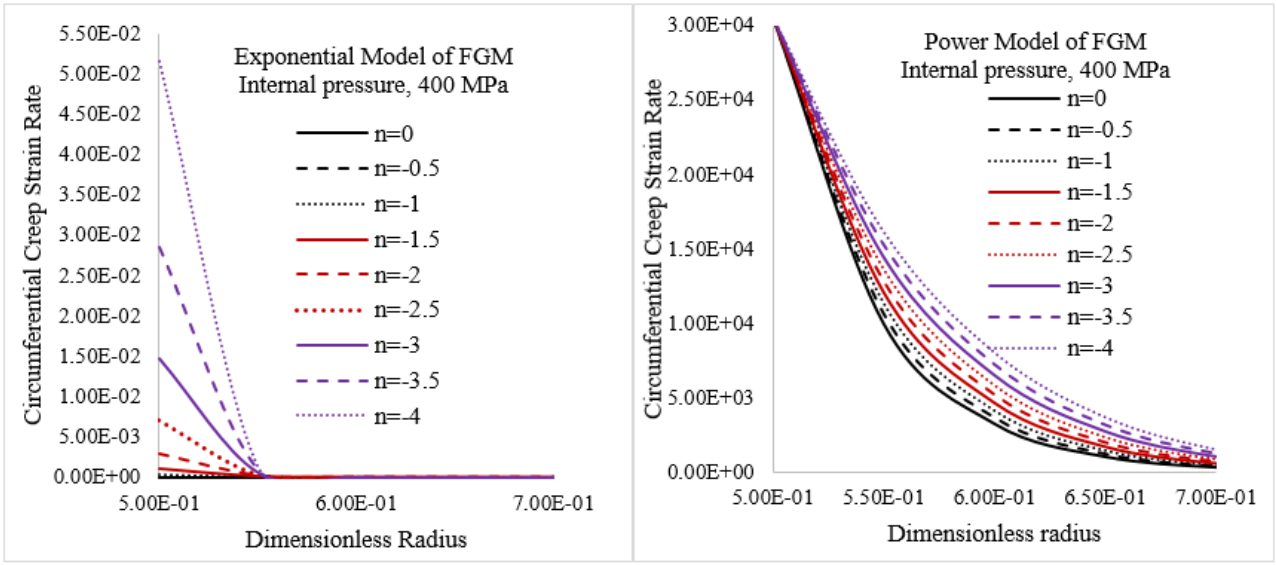

(a) *(b)*

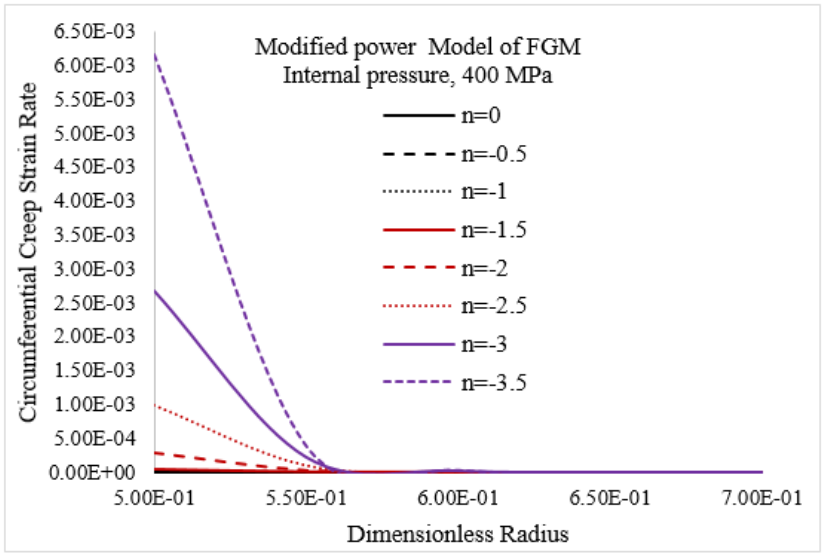

(c)

Figure 10. The changes in the rate of circumferential creep strain in terms of dimensionless radius for different *n*, *a*) the exponential model, *b*) the power model, and c) the modified power model (internal pressure, 400 MPa)

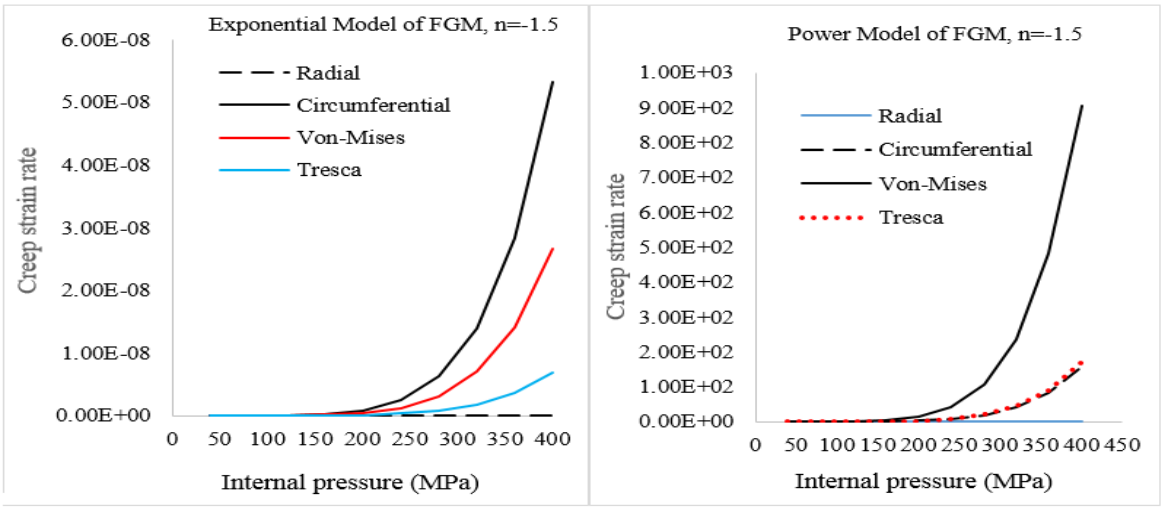

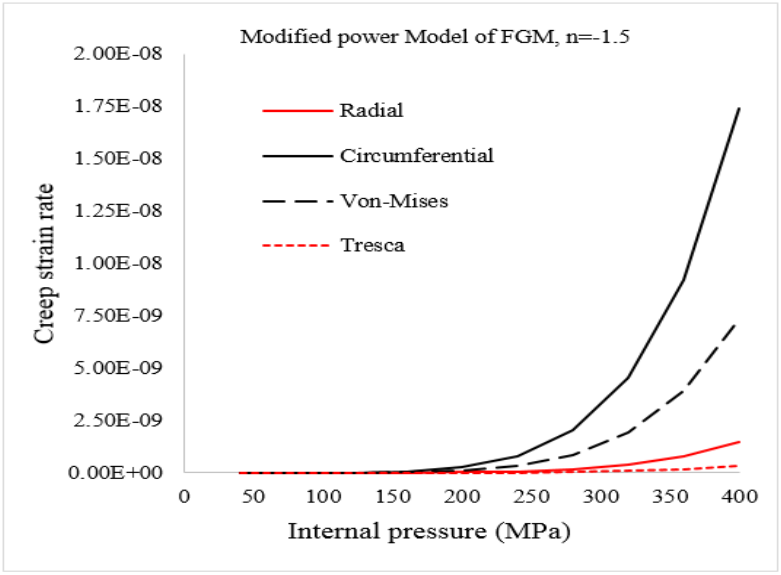

Figure 11. The changes in the rate of creep strains in terms of internal pressure, *a*) the exponential model, *b*) the power model, and c) the modified power model (*n*=-1.5, dimensionless mean radius)

For further discussion of the results of the three models of the present work, two new ratios in the following form were considered:

$$R_1 = R_{srain\ rate} = \frac{Radial\ creep\ strain\ rate}{Circumferential\ \ creep\ strain\ rate}, \quad R_2 = R_{eq} = \frac{Von{-}Mises\ creep\ strain\ rate}{Tresca\ \ creep\ strain\ rate}$$

According to Tables 1 and 2, the value of R_1, R_2 in terms of internal pressure for three models are illustrated. Although increasing internal pressure, radial, and circumferential creep strain rates increase, R_1, for three models, and R_2 for exponential and modified power models, remains almost constant which is an interesting and thought-provoking result.

Table. 1. Variation of radial, and circumferential creep strains rate, and R_1 in terms of internal pressure

Internal Pressure (MPa)	Radial Creep Strain Rate, *n*=-1.5			Circumferential Creep Strain Rate, *n*=-1.5			$R_{srain\ rate=}R_1$		
	FGM Models								
	Exponential	Power	Modified Power	Exponential	Power	Modified Power	Exponential ($\times10^{-4}$)	Power ($\times10^{-12}$)	Modified Power ($\times10^{-2}$)
40	3.15×10^{-17}	8.84×10^{-16}	1.45×10^{-15}	5.32×10^{-14}	1.57×10^{-04}	1.74×10^{-14}	5.92	5.63	8.33
80	2.02×10^{-15}	5.66×10^{-14}	9.28×10^{-14}	3.40×10^{-12}	1.01×10^{-02}	1.11×10^{-12}	5.94	5.60	8.36
120	2.30×10^{-14}	6.44×10^{-13}	1.06×10^{-12}	3.88×10^{-11}	1.15×10^{-01}	1.27×10^{-11}	5.93	5.60	8.35
160	1.29×10^{-13}	3.62×10^{-12}	5.94×10^{-12}	2.18×10^{-10}	6.44×10^{-01}	7.11×10^{-11}	5.92	5.62	8.35
200	4.92×10^{-13}	1.38×10^{-11}	2.27×10^{-11}	8.31×10^{-10}	$2.46\times10^{+00}$	2.71×10^{-10}	5.92	5.61	8.38
240	1.47×10^{-12}	4.12×10^{-11}	6.77×10^{-11}	2.48×10^{-09}	$7.34\times10^{+00}$	8.10×10^{-10}	5.93	5.61	8.36
280	3.70×10^{-12}	1.04×10^{-10}	1.71×10^{-10}	6.26×10^{-09}	$1.85\times10^{+01}$	2.04×10^{-09}	5.91	5.62	8.38
320	8.26×10^{-12}	2.32×10^{-10}	3.80×10^{-10}	1.39×10^{-08}	$4.12\times10^{+01}$	4.55×10^{-09}	5.94	5.63	8.35
360	1.67×10^{-11}	4.70×10^{-10}	7.71×10^{-10}	2.83×10^{-08}	$8.36\times10^{+01}$	9.23×10^{-09}	5.90	5.62	8.35
400	3.15×10^{-11}	8.84×10^{-10}	1.45×10^{-09}	5.32×10^{-08}	$1.57\times10^{+02}$	1.74×10^{-08}	5.92	5.63	8.33

Table. 2. Variation of radial, and circumferential creep strains rate in terms of internal pressure

Internal Pressure (MPa)	Von-Mises Creep Strain Rate, *n*=-1.5			Tresca Creep Strain Rate, *n*=-1.5			$R_{eq=}R_2$		
	FGM Models								
	Exponential	Power	Modified Power	Exponential	Power	Modified Power	Exponential ($\times10^{-4}$)	Power ($\times10^{-12}$)	Modified Power ($\times10^{-2}$)
40	2.66×10^{-14}	9.04×10^{-04}	7.34×10^{-15}	6.82×10^{-15}	1.70×10^{-04}	3.36×10^{-16}	3.90	5.32	21.8
80	1.70×10^{-12}	$5.79\times1^{0-02}$	4.70×10^{-13}	4.37×10^{-13}	1.09×10^{-02}	2.15×10^{-14}	3.89	5.31	21.9
120	1.94×10^{-11}	6.59×10^{-01}	5.35×10^{-12}	4.97×10^{-12}	1.40×10^{-02}	2.45×10^{-13}	3.90	47.1	21.8
160	2.18×10^{-10}	$3.70\times10^{+00}$	3.01×10^{-11}	1.09×10^{-10}	1.24×10^{-01}	1.38×10^{-12}	2.00	29.8	21.8
200	4.16×10^{-10}	$1.41\times10^{+01}$	1.15×10^{-10}	1.07×10^{-10}	6.98×10^{-01}	5.25×10^{-12}	3.89	20.2	21.9
240	1.24×10^{-09}	$4.22\times10^{+01}$	3.42×10^{-10}	3.18×10^{-10}	$7.95\times10^{+00}$	1.57×10^{-11}	3.90	5.31	21.8
280	3.13×10^{-09}	$1.06\times10^{+02}$	8.63×10^{-10}	8.03×10^{-10}	$2.00\times10^{+01}$	3.95×10^{-11}	3.90	5.30	21.8
320	6.98×10^{-09}	2.32×10^{-10}	3.80×10^{-10}	1.39×10^{-08}	$4.12\times10^{+01}$	4.55×10^{-09}	5.94	5.63	21.8
360	1.67×10^{-11}	4.70×10^{-10}	7.71×10^{-10}	2.83×10^{-08}	$8.36\times10^{+01}$	9.23×10^{-09}	5.90	5.62	8.35
400	3.15×10^{-11}	8.84×10^{-10}	1.45×10^{-09}	5.32×10^{-10}	$1.57\times10^{+02}$	1.74×10^{-08}	5.92	5.63	8.33

4. Conclusion

The analytical results of this study can be summarized as follows;

1. The variation of creep strains rate for exponential FGM model in internal radius with increasing *n* from -4 to 0, reduces as an exponential function. Also, the slope of the graph has

the highest value at a pressure of 360 MPa, and the changes in creep strain rate in terms of pressure remain constant.

2. In the power FGM model, considering mean radius and parameters changes (internal pressure: 40-400 MPa, n=-4-0), the creep strains rate decreases as an exponential function, and the slope of the graphs increases, and they have the lowest value on the outer wall of the vessel.
3. The advantage of the power FGM model compared to the exponential model is that in the inner radius for all n, the investigated parameters have a constant value, and this type of change is maintained by increasing the internal pressure value up to 400 MPa. The graphs are smooth, and their values tend to zero in the outer wall.
4. According to the results of the current research that have been obtained for different pressures, the Von Mises yield criterion can be used to discuss the selection of a reliable model.
5. According to Tables 1 and 2, although increasing internal pressure, radial, and circumferential creep strains rate increase, R_1, for all three models, and R_2 for exponential and modified power models, remains almost constant which is an interesting and thought-provoking result.

5. References

[1] Xu, Q., Yang, X. and Lu, Z. 2017. On the development of creep damage constitutive equations: A modified hyperbolic sine law for minimum creep strain rate and stress and creep fracture criteria based on cavity area fraction along grain boundaries. Materials at High Temperatures. 34(5-6): 323-332. doi: 10.1080/09603409.2017.1388603.

[2] Stewart, C.M. and Gordon, A.P. 2012. Constitutive modeling of multistage creep damage in isotropic and transversely isotropic alloys with elastic damage. Journal of Pressure Vessel Technology. 134(4): doi: 10.1115/1.4005946.

[3] Rouse, J.P., Sun, W., Hyde, T.H. and Morris, A. 2013. Comparative assessment of several creep damage models for use in life prediction. International Journal of Pressure Vessels and Piping. 108-109: 81-87. doi: 10.1016/j.ijpvp.2013.04.012.

[4] Mao, J.F., Zhu, J.W., Bao, S.Y., Luo, L.J. and Gao, Z.L. 2015. Creep and damage analysis of reactor pressure vessel considering core meltdown scenario. Procedia Engineering. 130: 1148-1161. doi: 10.1016/j.proeng.2015.12.283.

[5] Kan, K., Muránsky, O., Bendeich, P.J., Wright, R.N., Kruzic, J.J. and Payten, W. 2019. Assessment of creep damage models in the prediction of high-temperature creep behaviour of alloy 617. International Journal of Pressure Vessels and Piping. 177: 103974. doi: 10.1016/j.ijpvp.2019.103974.

[6] Habibi, N., Samawati, S. and Ahmadi, O. 2019. Transient thermal stresses analysis in a fpgm cylinder. Mechanics Of Advanced Composite Structures. 6(2): 81-94. doi: 10.22075/macs.2019.14988.1147.

[7] Houari, A., Madani, K., Amroune, S., Zouambi, L. and Elajrami, M. 2023. Numerical study of the mechanical behaviour and damage of FGM bent pipes under internal pressure and combined bending moment. Acta Mechanica et Automatica. 17(3): 460-468. doi:10.2478/ama-2023-0053.

[8] Abdolkhani, F., Hashemian, M., Aghadavoudi, F. and Habibi, N. 2023. Creep of autofrettaged thick-walled FGM cylindrical vessel. Proceedings of the Institution of Mechanical Engineers, Part

C: Journal of Mechanical Engineering Science. 09544062231185501. doi: 10.1177/09544062231185501.

[9] Zrinej, S., Laghzale, N. and Bouzid, H.A. 2023. Analytical modeling of shrink-fitted FGM thick-walled cylinder. International Journal of Engineering Research in Africa. 66: 61-74. doi: 10.4028/p-R5wvlY.

[10] Sklepus, S.M. 2022. Creep of complex-shaped bodies of revolution made of functionally gradient materials. International Applied Mechanics. 58: 464-471. doi: 10.1007/s10778-022-01171-0.

[11] Najibi, A. 2017. Mechanical stress reduction in a pressurized 2d-FGM thick hollow cylinder with finite length. International Journal of Pressure Vessels and Piping. 153: 32-44. doi: 10.1016/j.ijpvp.2017.05.007.

[12] Habibi, N., Samawati, S. and Ahmadi, O. 2016. Creep analysis of the FGM cylinder under steady-state symmetric loading. Journal of Stress Analysis. 1(1): 9-21. doi: 10.22084/jsa.2017.11195.1003.

[13] Yildirim, V. 2017. Exact Thermal Analysis of Functionally Graded Cylindrical and Spherical Vessels. International Journal of Engineering and Applied Sciences. 9(2): 112-126. doi: 10.24107/ijeas.318459.

[14] Aleayoub, S.M.A. and Loghman, A. 2010. Creep stress redistribution analysis of thick-walled FGM spheres. Journal of Solid Mechanics. 2(2): 115-128. dor: 20.1001.1.20083505.2010.2.2.2.0

[15] Celebi, K., Yarimpabuç, D. and Keles, I. 2017. A novel approach to thermal and mechanical stresses in a FGM cylinder with exponentially-varying properties. Journal of Theoretical and Applied Mechanics. 55(1): 343-351. doi: https://doi.org/10.15632/jtam-pl.55.1.343.

[16] Kalali, A.T., Moud, S.H. and Hassani, B. 2016. Elasto-plastic stress analysis in rotating disks and pressure vessels made of functionally graded materials. Latin American Journal of Solids and Structures. 13(5): 819-834. doi: 10.1590/1679-78252420.

[17] Jabbari, M., Bahtui, A. and Eslami, M.R. 2006. Axisymmetric mechanical and thermal stresses in thick long FGM cylinders. Journal of Thermal Stresses. 29(7): 643-663. doi: 10.1080/01495730500499118.

[18] Nagler, J. 2016. Radial body forces influence on FGM and non- FGM cylindrical pressure vessels. Journal of Composites. 2016: 3298685. doi: 10.1155/2016/3298685.

[19] Khanna, K., Gupta, V. and Nigam, S. 2015. Creep analysis of a variable thickness rotating FGM disc using tresca criterion. Defence Science Journal. 65: 163-170. doi: 10.14429/dsj.65.8045.

[20] Smaisim, G.F., Bidgoli, M.O., Goh, K.L. and Bakhtiari, H. Review of thermoelastic, thermal properties and creep analysis of functionally graded cylindrical shell. Australian Journal of Mechanical Engineering.): 1-12. doi: 10.1080/14484846.2022.2100045.

[21] Kiarasi, F., Babaei, M., Omidi Bidgoli, M., Reza Kashyzadeh, K. and Asemi, K. 2022. Mechanical characterization and creep strengthening of az91 magnesium alloy by addition of yttrium oxide nanoparticles. Proceedings of the Institution of Mechanical Engineers, Part L: Journal of Materials: Design and Applications. 236(8): 1489-1500. doi: 10.1177/14644207211073499.

[22] Koohi Faegh Dehkourdi, R., Omidi Bidgoli, M. and Hosseini, M. 2022. A case study on the influence of friction coefficient and rotational speed on transient thermoelastic response of FGM

rotating cylinder. Mechanics Of Advanced Composite Structures. 9(2): 399-408. doi: 10.22075/macs.2022.24906.1362.

[23] Seddighi, H., Ghannad, M. and Loghman, A. 2023. Creep behavior of cylinders subjected to an internal pressure and a two dimensional temperature field using first order shear deformation theory. Journal of Solid Mechanics. 15(3): 327-342. doi: 10.22034/jsm.2023.1977631.1764.

[24] Ahmed, J. A. 2017. Analytical solutions and multiscale creep analysis of Functionally Graded cylindrical pressure vessels. Louisiana State University and Agricultural and Mechanical College. doi: 10.31390/gradschool_dissertations.4279.

[25] Clyne, T.W. and Withers, P.J. 1993. An introduction to metal matrix composites. ed. Cambridge University Press, Cambridge.

[26] Nieh, T.G. 1984. Creep rupture of a silicon carbide reinforced aluminum composite. Metallurgical Transactions A. 15(1): 139-146. doi: 10.1007/BF02644396.

[27] Jahed, H. and Bidabadi, J. 2003. An axisymmetric method of creep analysis for primary and secondary creep. International Journal of Pressure Vessels and Piping. 80(9): 597-606. doi: 10.1016/S0308-0161(03)00136-4.

[28] Singh, S. and Rattan, M. 2010. Creep analysis of an isotropic rotating al-sic composite disc taking into account the phase-specific thermal residual stress. Journal of Thermoplastic Composite Materials. 23: 299-312. doi: 10.1177/0892705709345938.

[29] Chen, J.J., Tu, S.T., Xuan, F.Z. and Wang, Z.D. 2007. Creep analysis for a functionally graded cylinder subjected to internal and external pressure. The Journal of Strain Analysis for Engineering Design. 42(2): 69-77. doi: 10.1243/03093247JSA237.

[30] Garg, M., Deepak, D. and Gupta, V.K. 2014. Fe modeling of creep in linear and non-linear FGM cylinder under internal pressure. Multidiscipline Modeling in Materials and Structures. 10(1): 94-105. doi: 10.1108/MMMS-10-2012-0016.